

Numerical Investigation for the Bearing Performance of the Segmental Joint with Elastic Gasket

Ming Huang¹, Xinhua Shi¹, Fan Yang^{1*}, Kang Liu¹

¹ School of Civil Engineering, Hefei University of Technology, Hefei 230009, China

* Corresponding author, e-mail: fyang@hfut.edu.cn

Received: 25 February 2022, Accepted: 28 July 2022, Published online: 17 August 2022

Abstract

Detailed three-dimensional numerical models considering concrete indentation, bolts, elastic gasket (EG) and sealing gasket (SG) are established for the segmental joint with gaskets, and the load tests of the joints with EG and without EG are simulated and compared. The results reveal that the bearing performance of the joint with EG is very complex. In sagging moment scenarios, it can be divided into four stages by three key points “EG starts to open”, “joint external edge starts to contact” and “EG fully opened”. In hogging moment scenarios, it can be divided into three stages by two key points “SG opened” and “EG starts to open”. The EG has a significant effect on the joint bearing performance. It can soften the joint, which leads to the result that the average bending stiffness and ultimate bearing capacity of the joint with EG are evidently smaller and weaker than those of the joint without EG. With decreasing the joint axial force, this softening effect tends to be more obvious. Besides, for the two joints, the ultimate states of the joints subject to the bending moments are both that the concrete at the joint edges yields firstly, and it is necessary to protect or strengthen the corresponding concrete.

Keywords

shield water conveyance tunnel, segmental joint, bearing performance, elastic gasket, finite element model

1 Introduction

In recent years, with the massive construction of the inter-basin and long-distance water diversion projects in China, the shield method has been widely used in hydraulic pressure tunnels such as the water conveyance tunnel for the Qingcaosha Water Conveyance Project [1], the Yellow River Crossing Tunnel for the Middle Route of South-to-North Water Transfer Project [2], the water conveyance tunnel for the water allocation project in Pearl River Delta [3], etc. The segmental lining, which is adapted for shield tunnels, generally consists of several segments connected by bolts, sealing gasket (SG), elastic gasket (EG), etc. Whether there are gaskets is an important characteristic to distinguish the structure types of the segmental joints. Unlike highway tunnels or railway tunnels, the segmental lining for the water conveyance tunnel needs to bear not only external pressure but also internal water pressure. In addition, it also needs to ensure the quality and quantity of the conveyed water. Therefore, as shown in Fig. 1, several materials (e.g., SG and EG) are packed in the segmental joint to enhance the anti-seepage, alleviate the stress concentration, improve the flatness of the contact surface, etc. [4–6].

In some analytical and numerical researches, the bearing performance of the segmental joint for a shield tunnel lining is commonly simulated by three kinds of stiffnesses, which are rotational stiffness, axial stiffness and shear stiffness [7, 8]. Since the axial stiffness and shear stiffness contribute little to the bearing performance of the segmental joint, they can be simplified or even ignored in structure analyses [9]. However, the rotational stiffness has a significant influence on the bearing performance of the segmental joint, and it is a key parameter to be considered in the structural design of the segmental lining [9, 10]. Therefore, in recent years, an enormous amount of research effort goes into the joint rotational stiffness from the aspects of experimental tests, numerical simulations and theoretical analyses. These researches indicate that the mechanical behavior and bearing performance of the segmental joint subject to bending moments and axial forces are very complex, and the joint rotational stiffnesses present obvious nonlinear characteristics with the influences of the complexity and diversity of segment joint types, structural dimensions and involved materials [11–15].

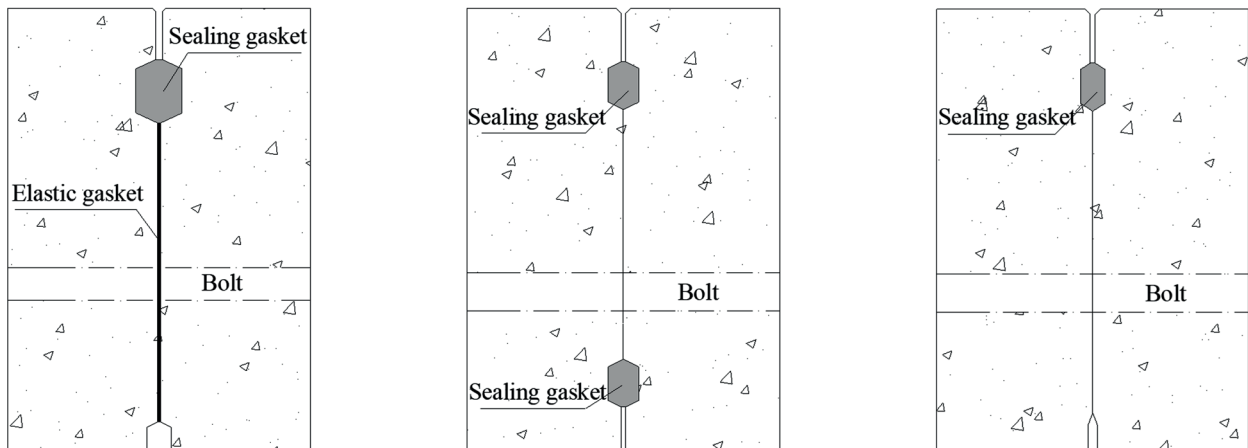


Fig. 1 Sketch of some segmental joints: (a) Joint of the Yellow River Crossing Tunnel; (b) Joint of the Qingcaosha water conveyance tunnel; (c) Joint of the of Shanghai Metro Line No. 13 tunnel

Currently, the existing experimental test and numerical simulation researches on the segmental joints mainly focused on the segmental joints without any EG. The bearing performance of the segmental joint with EG has not been fully clarified, and the bearing performances of the joint with EG and the joint without EG have not been compared in detail. Some relevant researches only reveal that the SG has a negligible influence on the joint bearing performance [12, 14]. However, the influence of EG on the joint bearing performance has not been clarified. In terms of theoretical analyses, the existing analytical models for calculating the rotational stiffness of the joint with EG are mainly based on the assumption that the concrete is much more rigid than EG, and the deformations of EG are much greater than that of the concrete. Therefore, only the compressive strains of EG are taken into consideration, while the compressive strains of the concrete attached to the EG are neglected [16–19]. In sum, this assumption only takes into account the stress generated by the compression of the EG structure instead of the concrete-EG-concrete composite structure. However, according to the constitutive model of EG, the rigidity of the EG tends to be increased rapidly with increasing the compressive stress, and the EG can no longer be considered as a flexible material in this condition [20–22]. In view of the complexity of the EG materials, further studies will be needed to clarify the bearing performance of this segmental joint with fully consideration of the role of EG.

This study is absorbed in the bearing performance of the segmental joint with EG which is commonly used in the shield water conveyance tunnel. According to the detailed structural characteristics of the segmental joint

with EG, a detailed three-dimensional (3D) finite element model considering the concrete indentation, bolt, SG and EG is established. Based on the numerical loading tests, the bearing performance of the segmental joint with EG is analyzed and compared with that of the segmental joint without EG, and the effect of EG on the bearing performance of the segmental joint is clarified.

2 Numerical models

2.1 Dimensions

The segmental joint with EG for the segmental lining of the Yellow River Crossing Tunnel is adopted as a case study, and its detailed structures and dimensions are presented in Fig. 2. The segment is made of C50 concrete and its yield strength is 32.4 MPa. The segment thickness is 0.4 m, and the width is 1.6 m. The segmental joint is formed by connecting adjacent segments using four M30 bolts with a yield strength of 420 MPa, and each bolt is applied with a pre-tightening force of 100 kN. A SG and a EG are packed in the segmental joint. The thickness of the EG is 1.5 mm. For the segmental joint without EG, the dimensions and materials of the concrete, bolts and SG are all the same as the segmental joint with EG, and the only difference is that it does not contain EG.

2.2 Materials

2.2.1 Concrete

A multilinear isotropic hardening material model and the von Mises yielding criterion are adapted for the concrete. The stress-strain relationship can be calculated by using the following equations [23]:

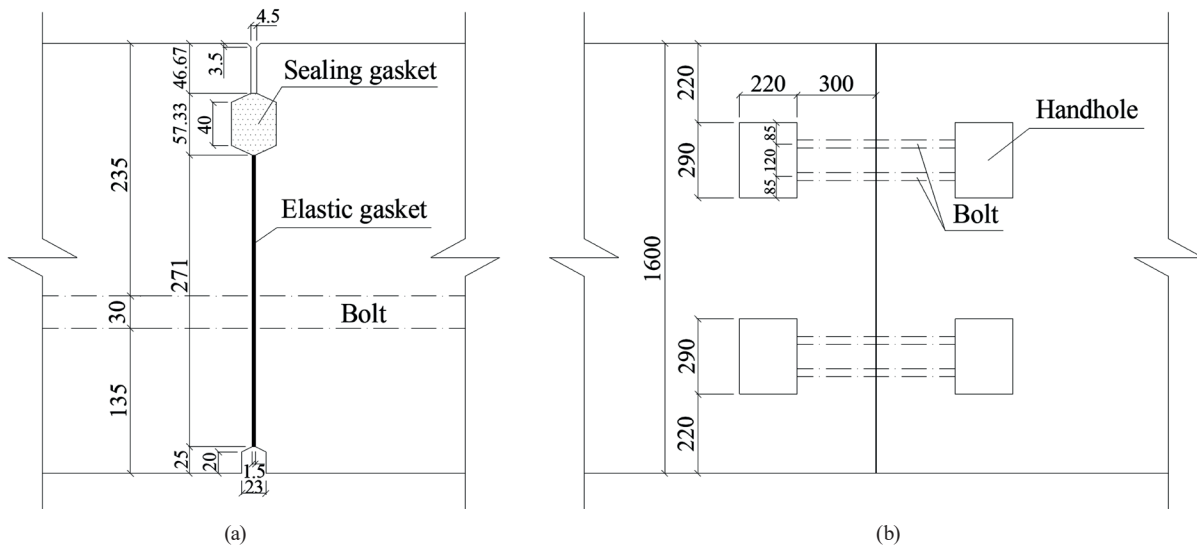


Fig. 2 Segmental joint with EG (mm): (a) Front view; (b) Bottom view (mm)

$$\sigma_c = \frac{\rho_c n}{n-1+x^n} E_c \varepsilon_c, \tag{1}$$

$$\rho_c = \frac{f_{c,r}}{E_c \varepsilon_{c,r}}, \tag{2}$$

$$n = \frac{E_c \varepsilon_{c,r}}{E_c \varepsilon_{c,r} - f_{c,r}}, \tag{3}$$

$$x = \frac{\varepsilon_c}{\varepsilon_{c,r}}, \tag{4}$$

where σ_c is the compressive stress; ε_c is the strain; E_c is the elastic modulus; and $f_{c,r}$ is the characteristic value of the axial compressive strength at the strain $\varepsilon_{c,r}$.

2.2.2 Bolt

A bilinear kinematic hardening material model is used for the bolt, and the stress-strain relationship can be calculated by using the following equations:

$$\sigma_b = \begin{cases} E_b \varepsilon_b & (\varepsilon_b < \varepsilon_b') \\ f_b + E_b' (\varepsilon_b - \varepsilon_b') & (\varepsilon_b \geq \varepsilon_b') \end{cases}, \tag{5}$$

where σ_b is the stress at any strain ε_b ; E_b is the elastic modulus; E_b' is the plastic modulus which is considered as $0.01 E_b$; f_b is the yield stress; and ε_b' is the yield strain.

2.2.3 Gasket

There are two gaskets involved in the segmental joint. The SG and EG are generally made of ethylene propylene diene monomer and nitrile butadiene rubber, respectively. According to the compressive experiments [20, 24], the material models of the two gaskets can be expressed as

$$F_s = 938.8 \Delta_s^2 + 2623.2 \Delta_s, \tag{6}$$

$$\sigma_e = 248 \varepsilon_e^{1.67}, \tag{7}$$

where F_s is the compressive force on the sealing gasket per meter (N); Δ_s is the compressive deformation of the sealing gasket (mm); σ_e is the compressive stress of the EG (MPa); and ε_e is the strain of the EG.

2.3 Detailed 3D numerical model

The 3D finite element analysis software ANSYS is used to establish detailed 3D finite element models for the segmental joint with EG and the segmental joint without EG, respectively, as shown in Fig. 3. For the segmental joint with EG, 3D solid elements (SOLID 65) are used for the concrete, and 3D solid elements (SOLID 45) are used for the bolt and SG. The EG is simulated using 3D interface elements (INTER 195) which can only be compressed in the normal direction. The contact interactions including the interaction between the concrete and bolt, the interaction between the concrete and SG and the interaction between the segment edges are simulated by "face-to-face" contact elements. In most cases, the concrete friction coefficients range from 0.2 to 0.5 [25, 26], and an average value of 0.35 is adopted in the simulation.

For the segmental joint without EG, the numerical model of the concrete, bolts and SG are exactly the same as the model of the segmental joint with EG. The only difference is that it does not contain EG, and the corresponding concrete is compressed by contacts.

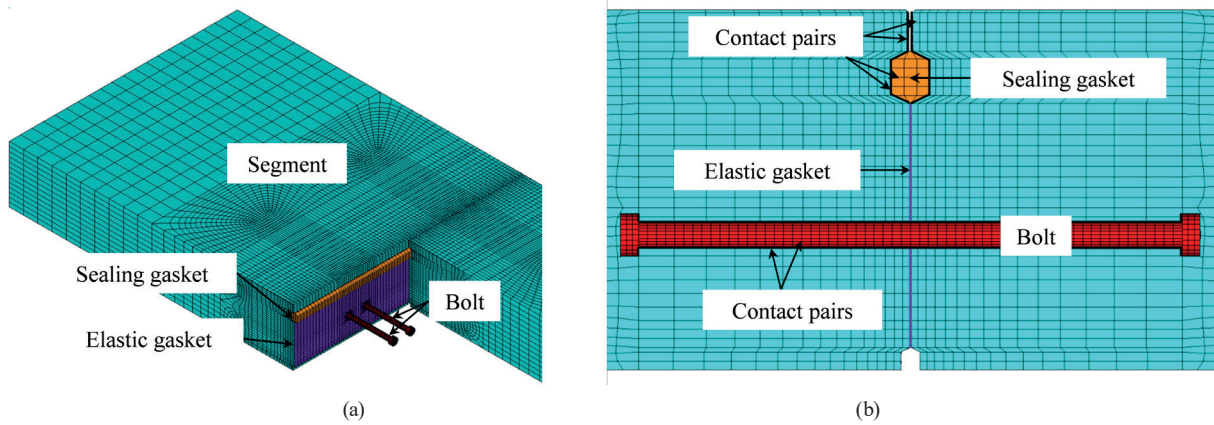


Fig. 3 Detailed 3D finite element model of the segmental joint with EG: (a) Entirety; (b) Details

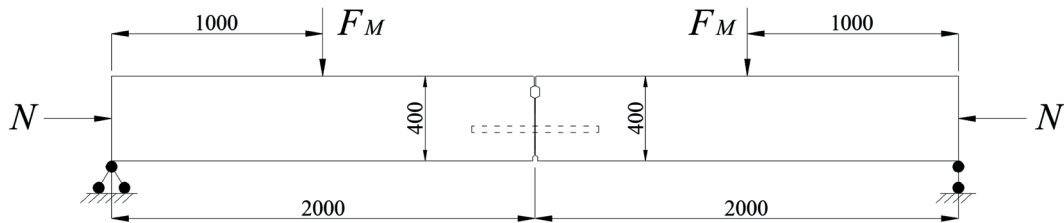


Fig. 4 Sketch of the bending test for the joint (mm)

3 Numerical loading tests

3.1 Test method

Loading tests performed by experimental or numerical methods are commonly used to obtain the rotational stiffness of the segmental joint. During the loading test, the curved segments can be replaced by the straight segments to simplify the tests and corresponding computations [11, 13, 27, 28]. The test scheme is presented in Fig. 4. A fixed support is positioned on the left end of the model, and a roller support is positioned on the right end. The joint axial forces are reproduced by the horizontal force (N), and the bending moments are reproduced by the vertical force (F_M).

When the joint is subject to the axial force and bending moment, the joint rotates, which leads to the result that the joint internal edge or external edge is open (Fig. 5). In most loading tests for the segmental joint, the joint rotation angles are calculated by monitoring the deformations of the joint external edges (points a and b) and joint internal edges (points c and d). For example, in the sagging moment scenario, the joint rotation angle can be obtained by the following equation:

$$\theta = \frac{S_{cd} - S_{ab}}{H}, \quad (8)$$

where θ is the joint rotation angle; S_{cd} is the averaged deformation of the joint internal edges; S_{ab} is the averaged deformation of the joint external edges; and H is the segment thickness.

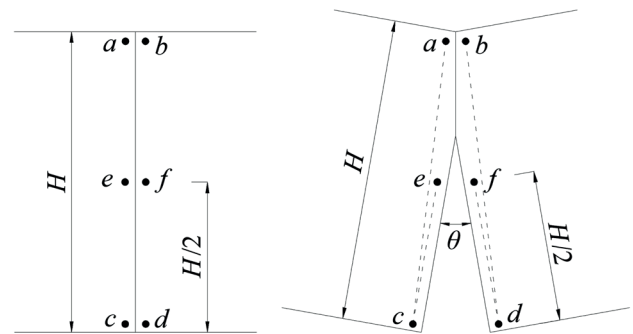


Fig. 5 Sketch of the joint rotation angle

However, the above calculation method of the joint rotation angle is based on the assumption that the joint interface is considered as a plane surface throughout the joint deformations. In these circumstances, the joint rotation angle calculated by Eq. (8) is smaller than the actual value.

Therefore, to reduce the errors of the calculation results, it is suggested to monitor the deformations of the joint centres (points e and f) during the test, and the rotation angles of a segmental joint subject to sagging moment and hogging moment can be calculated by Eq. (9) and Eq. (10), respectively. Then, according to the calculation results, the rotation angle versus the bending moment curves can be obtained. According to Eq. (11), the joint rotational stiffness (K_θ) can be obtained by the slope of the joint rotation angle (θ) versus the bending moment (M) curve.

$$\theta_s = \frac{S_{cd} - S_{ef}}{H/2}, \tag{9}$$

$$\theta_h = \frac{S_{ab} - S_{ef}}{H/2}, \tag{10}$$

$$K_\theta = \frac{M}{\theta}, \tag{11}$$

where θ_s is the joint rotation angle corresponding to the sagging moment; θ_h is the joint rotation angle corresponding to the hogging moment; S_{ef} is the averaged deformation of the joint centres; and H is the segment thickness.

3.2 Loading

Normally, when a segmental lining is subject to stable external or internal loads, the axial forces of these joints of the lining are more or less the same, while the bending moments are quite different. Therefore, the loading tests focus on the bearing performance of the segmental joint with a fixed axial force from the beginning of bending to the ultimate failure.

The loading process consists of the following three steps. For the first step, since the sealing gasket and elastic gasket are compressed and deformed in the initial stage under the action of penetrating bolts, apply the pre-tightening force to the bolt to simulate this state in this step. For the second step, by estimating the axial forces of the case studied lining under the actual conditions, the axial forces of the segments are about 2500 kN, and then apply the axial force (N) to the numerical models of the segments. For the third step, applying incremental vertical load (F_M) to the segment by multiple substeps until the joint failure, and the vertical load of each substep is 20 kN.

3.3 Ultimate limit state

According to some experimental results, the joint is damaged mainly because of the cracked concrete near the joint edges or the yield bolts [12, 13, 29, 30]. Therefore, in the numerical loading tests, the joint ultimate limit state is that either the concrete or the bolt begins to yield, and then the ultimate bearing capacities of the segmental joint with EG and the segmental joint without EG can be obtained, respectively.

4 Results and discussion

4.1 Sagging moment scenario

4.1.1 Segmental joint with EG

As seen from Figs. 6 to 8, according to the stress states of the concrete, SG and EG, the bearing performance of the segmental joint with EG can be divided into four stages by three key points "EG starts to open", "joint external edge starts to contact" and "EG fully opened" in the sagging moment scenario.

Stage 1: When $M \leq 120$ kN·m, the SG and EG are in compressed states, and the concrete near the joint external edge is not in contact. In this stage, there is no obvious deformation of the joint, and the joint rotation angles are much small. According to the relationship between the rotation angle and the sagging moment, the rotation stiffness of the joint in this stage is relatively large.

Stage 2: When 120 kN·m $< M \leq 280$ kN·m, the SG is compressed, and the concrete near the joint external edge is not in contact. However, the EG starts to open from its internal edge, and with increasing the sagging moment, the joint opening tends to be obvious. According to the relationship between the rotation angle and the sagging

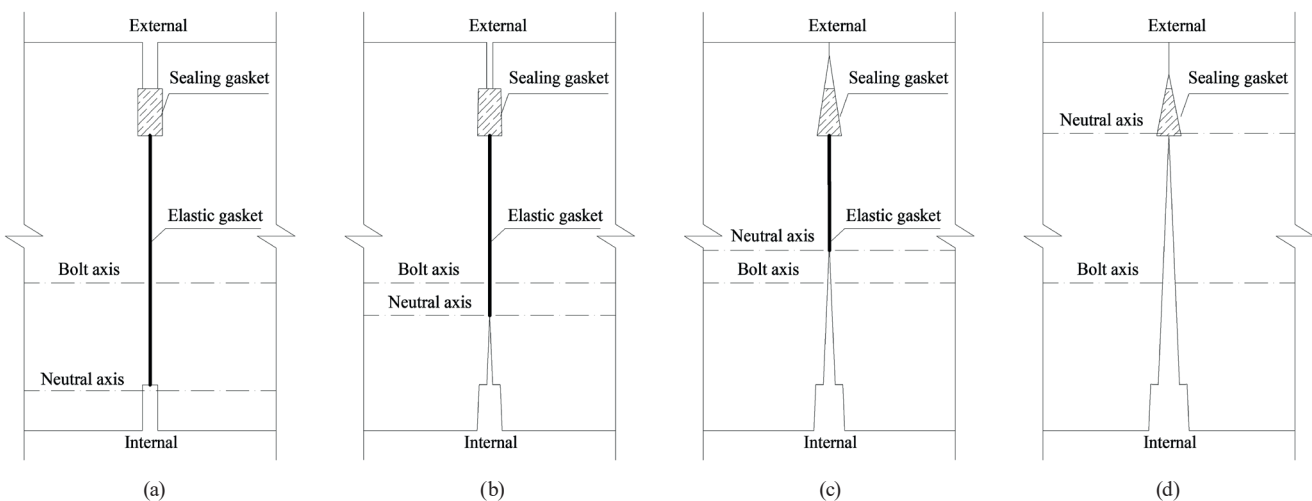


Fig. 6 Deformations of the segmental joint with EG in sagging moment scenario; (a) Stage 1, (b) Stage 2, (c) Stage 3, (d) Stage 4

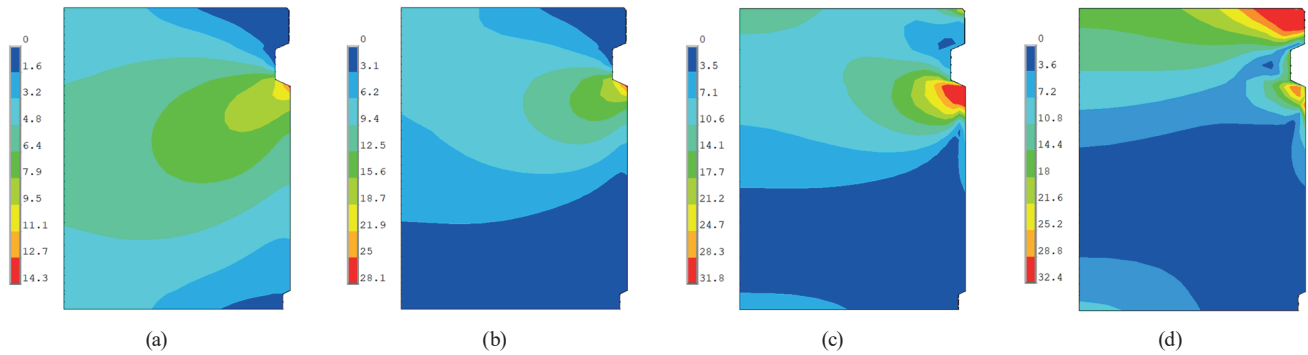


Fig. 7 Von Mises stresses of the segmental joint with EG in sagging moment scenario (MPa); (a) Stage 1 ($M = 60$ kNm), (b) Stage 2 ($M = 200$ kNm), (c) Stage 3 ($M = 360$ kNm), (d) Stage 4 ($M = 560$ kNm)

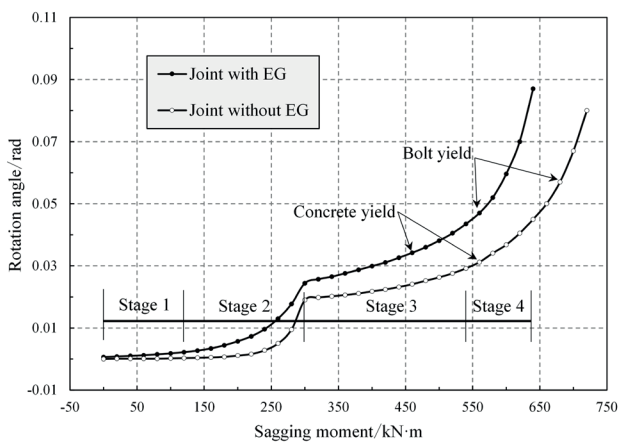


Fig. 8 Joint rotation angle versus sagging moment

moment, with increasing the sagging moment, the joint rotation stiffness is decreased gradually, and resulting in an obvious increase of the joint rotation angle.

Stage 3: When $280 \text{ kN}\cdot\text{m} < M \leq 540 \text{ kN}\cdot\text{m}$, the SG is compressed, and the EG is still partially compressed. While, in this stage, the concrete at the joint external edge starts to contact, and the concrete gradually yields from the external to internal with increasing the sagging moment. According to the relationship between the rotation angle and the sagging moment, the joint rotation stiffnesses in this stage are noticeably larger than those in the previous stage. It is because the concrete contact stresses begin to contribute to the restriction of the joint deformation, and it can significantly decrease the joint opening rate.

Stage 4: When $M > 540 \text{ kN}\cdot\text{m}$, the SG is compressed, the contact area of the joint external edge is further increased, and almost the whole EG is fully opened. According to the relationship between the rotation angle and the sagging moment, with increasing the sagging moment, the joint rotation stiffness is decreased gradually, while the joint opening rate is increased gradually. It is because, in this stage, the bolt begins to yield, and the concrete

yield region gradually expands from the joint external edge, which eventually results in the increase of the joint opening rate and the failure of the joint.

4.1.2 Segmental joint without EG

The deformations and stresses of the segmental joint without EG in the sagging moment scenario are presented in Figs. 9 and 10, respectively. Comparing Fig. 9 and Fig. 6, it can be seen that the bearing performance of the segmental joint without EG is similar to that of the joint with EG, and it can also be divided into four stages. For the joint with EG, the EG gradually opens from Stage 1 to Stage 3. For the joint without EG, it is the concrete contact surface gradually opens from Stage 1 to Stage 3. Therefore, comparing the joint rotation angle versus sagging moment curves of the two joints (Fig. 8), the shapes and trends of the two curves are similar separately. However, when the two joints are subject to the same sagging moment, the rotation angle of the joint with EG is evidently larger than that of the joint without EG. In addition, with increasing the sagging moment, the spacing between the two curves tends to be increased. Besides, comparing Fig. 10 and Fig. 7, when the two joints are subject to the same sagging moment in Stage 1 to Stage 3, the concrete maximum stress of the joint with EG is smaller than that of the joint without EG. This is because the EG can play a role in alleviating the concrete stress concentration. However, in Stage 4, the concrete of the joint with EG yields earlier, and with increasing the sagging moment, the yield region of the joint with EG is slightly larger than that of the joint without EG.

According to the above discussions, the EG has a significant effect on softening the joint, and with increasing the bending moment, the softening effect tends to be more obvious. According to Eq. 11 and Fig. 8, the average rotational stiffness of each joint can be calculated by the average value of the slopes at these substeps. Compared

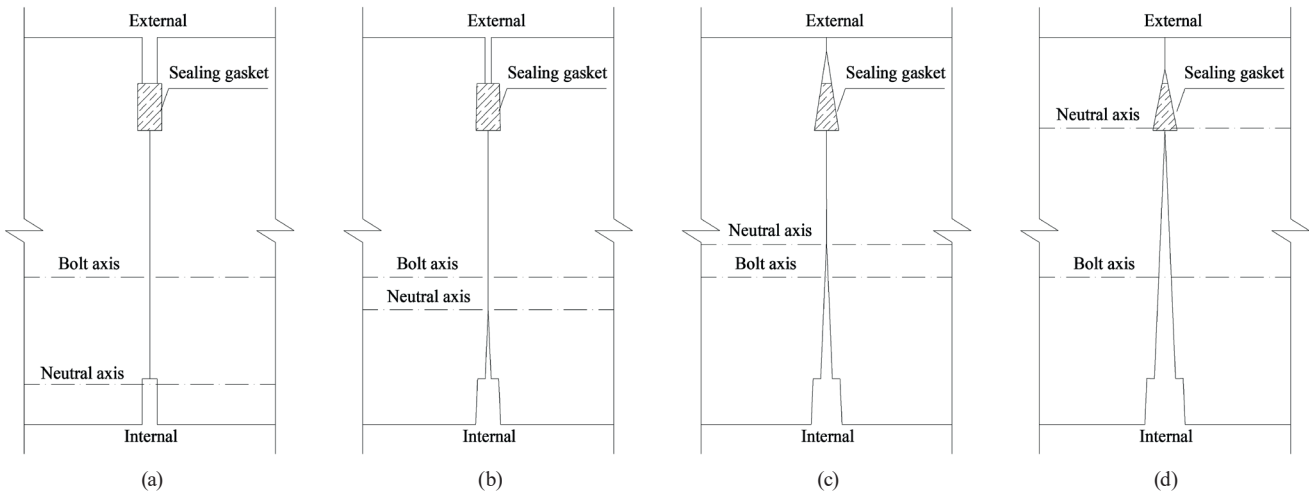


Fig. 9 Deformations of the segmental joint without EG in sagging moment scenario; (a) Stage 1, (b) Stage 2, (c) Stage 3, (d) Stage 4

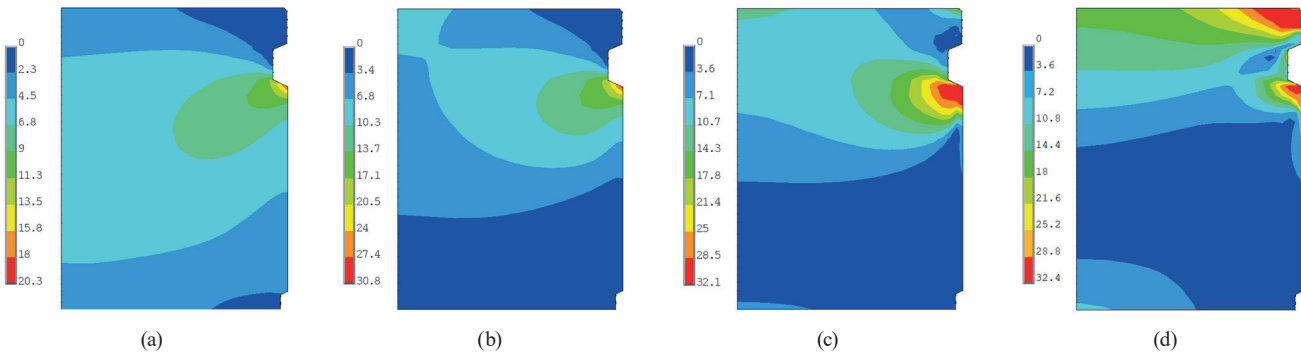


Fig. 10 Von Mises stresses of the segmental joint without EG in sagging moment scenario (MPa); (a) Stage 1 ($M = 60$ kNm), (b) Stage 2 ($M = 200$ kNm), (c) Stage 3 ($M = 360$ kNm), (d) Stage 4 ($M = 560$ kNm)

with the joint without EG, with the softening effect of the EG, the average rotational stiffness of the joint with EG is decreased by about 55%. In addition, the opening rate of the joint without EG is significantly increased, which leads the concrete and bolt to yield earlier. Thus, compared with the joint without EG, the ultimate bearing capacity of the joint with EG is decreased by about 18%.

4.2 Hogging moment scenario

4.2.1 Segmental joint with EG

As seen from Figs. 11 to 13, according to the stress states of the SG and EG, the bearing performance of the joint with EG can be divided into three stages by the two key points "SG opened" and "EG starts to open" in the hogging moment scenario.

Stage 1: When $M \leq 220$ kN·m, both the SG and EG are in compressed states. The joint deformation and stress state in this stage are similar to those in Stage 1 of the sagging moment scenario. In this stage, the joint rotation angle is small, the joint opening is negligible, and the joint rotation stiffness is relatively large.

Stage 2: When 220 kN·m $< M \leq 300$ kN·m, the joint starts to open from the external edge, the SG is no longer compressed, and the EG is still entirely compressed. According to the relationship between the rotation angle and the hogging moment, the joint rotation stiffness is still relatively large, which is similar to that in the previous stage. It also indicates that the SG has a negligible influence on the joint rotation stiffness.

Stage 3: When $M > 300$ kN·m, the EG starts to open from its external edge, and it is partially compressed. With increasing the hogging moment, the contact surface between the concrete and EG is decreased gradually, which leads to the result that the compressive stress of the corresponding concrete gradually increases and tends to yield from the joint internal edge. According to the relationship between the rotation angle and the hogging moment, the joint rotation stiffness gradually becomes smaller, the bolt begins to yield, and the concrete yield region expands from the joint internal edge, and at last the joint is damaged.

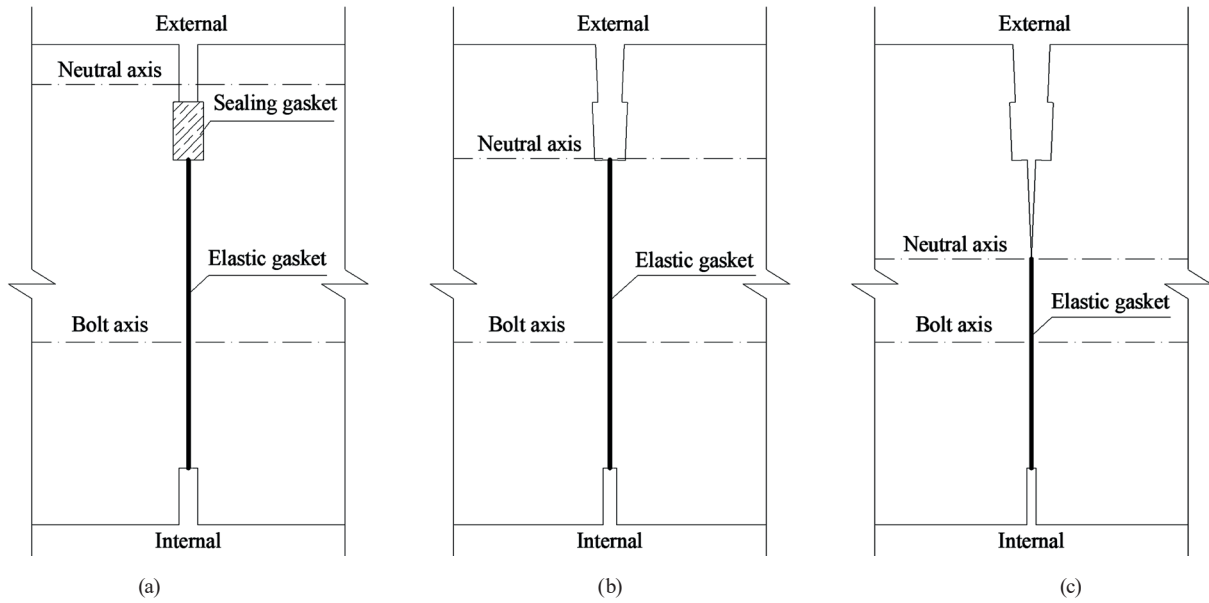


Fig. 11 Deformations of the segmental joint with EG in hogging moment scenario; (a) Stage 1, (b) Stage 2, (c) Stage 3

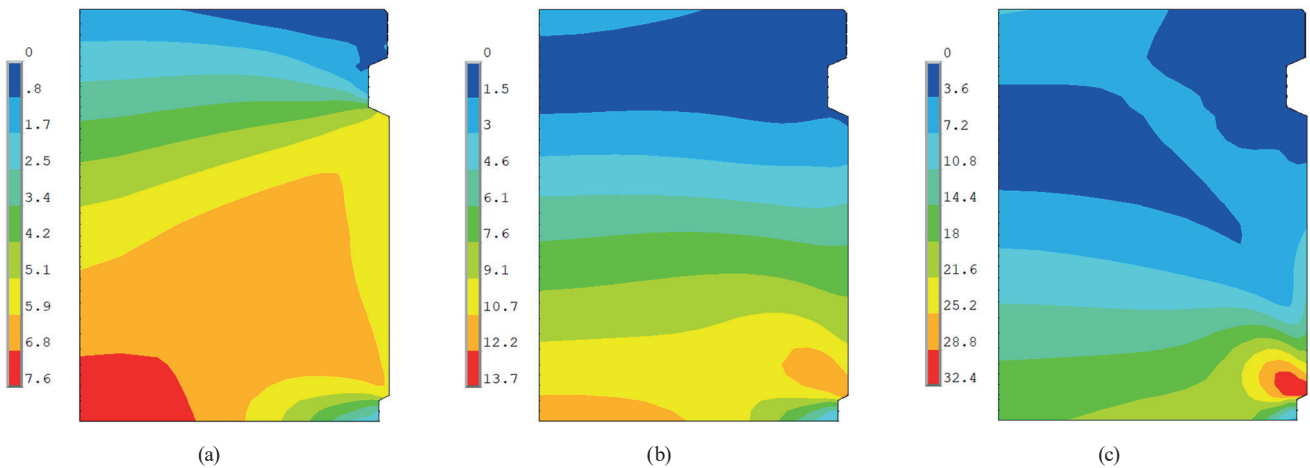


Fig. 12 Joint rotation angle versus hogging moment; (a) Stage 1 ($M = 80$ kNm), (b) Stage 2 ($M = 240$ kNm), (c) Stage 3 ($M = 440$ kNm)

4.2.2 Segmental joint without EG

The deformations and stresses of the segmental joint without EG in the hogging moment scenario are presented in Figs. 14 and 15, respectively. Comparing Fig. 14 and Fig. 11, the bearing performances of the two kinds of the segmental joints are similar, and both can be divided into three stages. For the joint without EG, the joint axial force and hogging moment are borne mainly by the contacted concrete, and the contact surface gradually opens from Stage 1 to Stage 3. Comparing Fig. 15 and Fig. 12, with the impact of the same hogging moment in Stage 1 to Stage 2, since the EG can alleviate the concrete stress concentration, the concrete maximum stress of the joint with EG is smaller than that of the joint without EG. However, in Stage 3, the concrete and bolt of the joint with EG yield

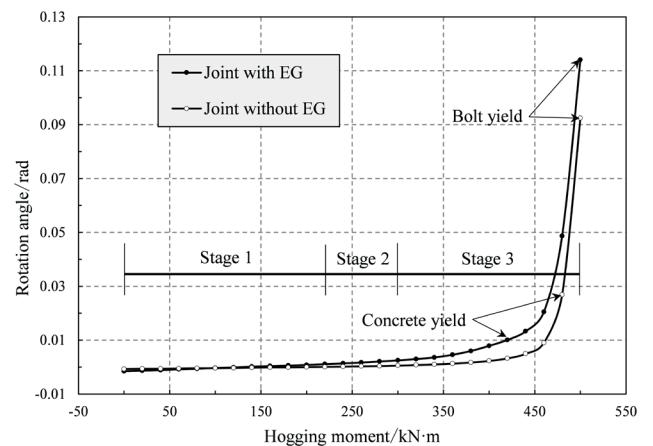


Fig. 13 Deformations of the segmental joint without EG in hogging moment scenario

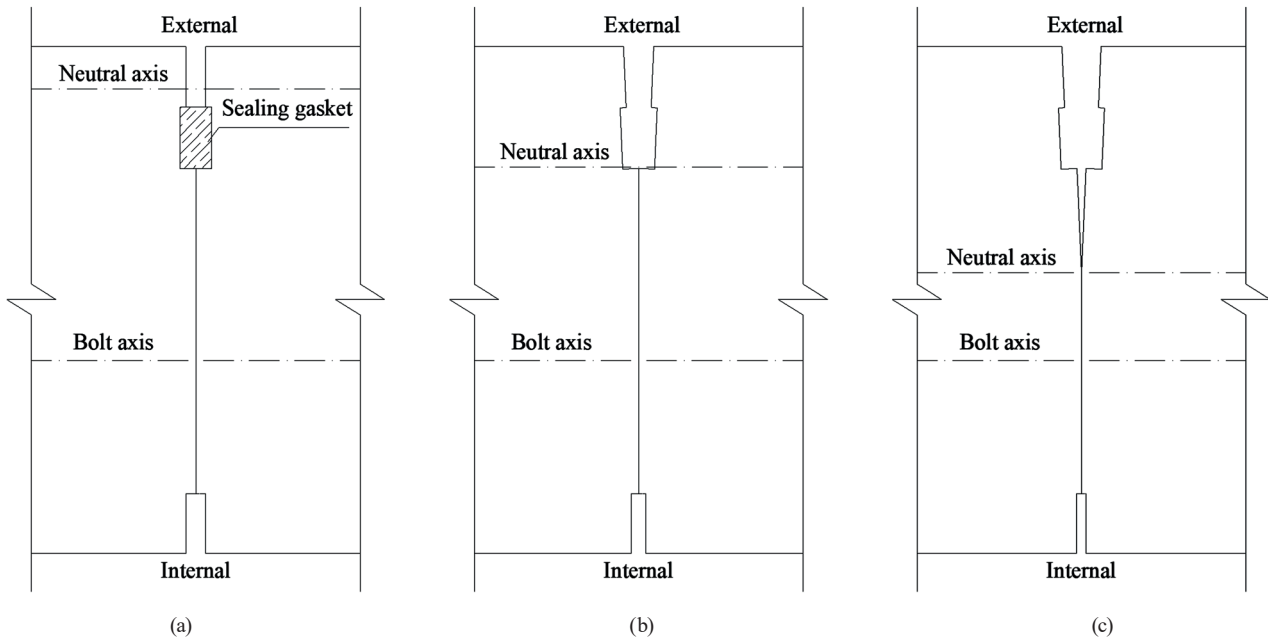


Fig. 14 Von Mises stresses of the segmental joint without EG in hogging moment scenario (MPa); (a) Stage 1, (b) Stage 2, (c) Stage 3

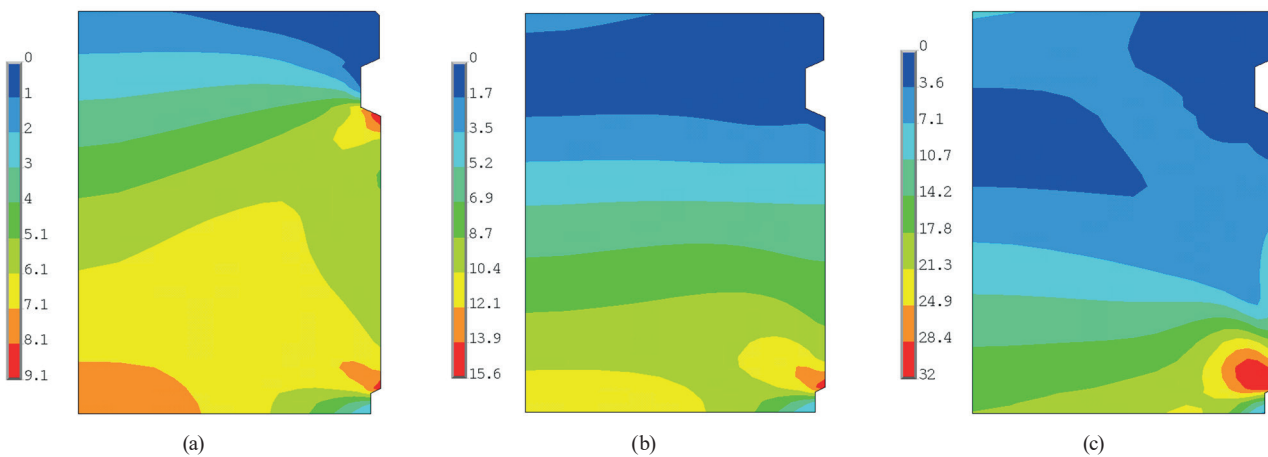


Fig. 15 Von Mises stresses of the segmental joint with EG in hogging moment scenario (MPa); (a) Stage 1 ($M = 80$ kNm), (b) Stage 2 ($M = 240$ kNm), (c) Stage 3 ($M = 440$ kNm)

earlier than those of the joint without EG. In addition, with the softening effect of the EG on the joint, the average rotational stiffness of the joint with EG calculated by Eq. 11 and Fig. 12 is decreased by about 56%, which leads to the fact that the deformations of the joint with EG are larger than that of the joint without EG, and the ultimate bearing capacity of the joint with EG is decreased by about 13%.

4.3 Influence of the axial force

The axial force of the joint has always been an important parameter affecting the joint rotational stiffness [9, 12]. As shown in Fig. 16 and Fig. 17, with decreasing the axial force, the rotational stiffnesses of the two joints both tend

to be significantly decreased. Besides, with the condition of different axial forces, the rotation angle versus bending moment curves of the two joints still conform to the above results that the curves can be divided into four stages in the sagging moment scenario and three stages in the hogging moment scenario. Meanwhile, with the condition of the same axial force, since the EG have a softening effect on the joint behavior, the average rotational stiffness of the joint with EG is smaller than that of the joint without EG. In addition, with decreasing the axial force, the average distance between the curves of the two joints subject to the same axial force is increased gradually, which indicates that the softening effect tends to be more significant.

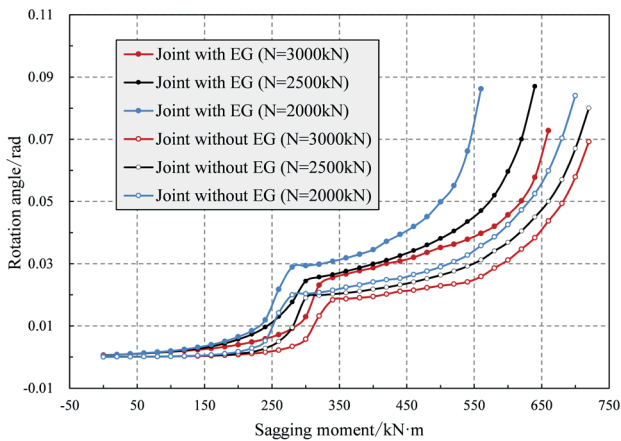


Fig. 16 Influence of axial forces on the rotation angle versus sagging moment

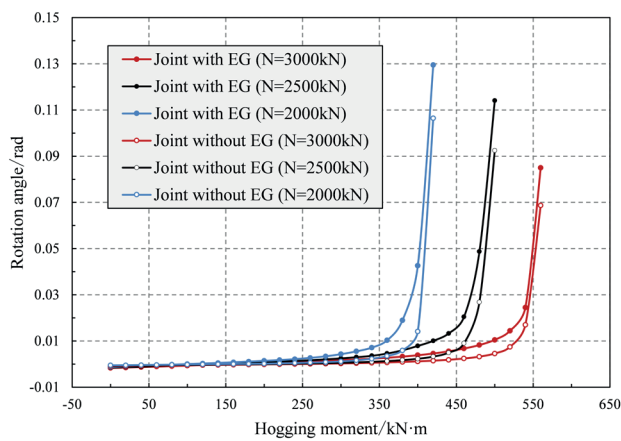


Fig. 17 Influence of axial forces on the rotation angle versus hogging moment

5 Conclusions

Detailed three-dimensional numerical models considering the stress conditions of the concrete, bolt, EG and SG are established to perform the loading tests of the segmental joint with EG and segmental joint without EG. By analyzing and comparing the bearing performance and progressive failure of the two joints, the following conclusions are obtained.

References

[1] Yu, H., Yuan, Y., Qiao, Z., Gu, Y., Yang, Z., Li, X. "Seismic analysis of a long tunnel based on multi-scale method", *Engineering Structures*, 49, pp. 572–587, 2013. <https://doi.org/10.1016/j.engstruct.2012.12.021>

[2] Yang, F., Cao, S., Qin, G. "Mechanical behavior of two kinds of prestressed composite linings: A case study of the Yellow River Crossing Tunnel in China", *Tunnelling and Underground Space Technology*, 79, pp. 96–109, 2018. <https://doi.org/10.1016/j.tust.2018.04.036>

1. The bearing performance of the segmental joint with EG is very complex, and it presents obvious nonlinear characteristics. In the sagging moment scenario, the bearing performance of the joint with EG can be divided into four stages by the three key points "EG starts to open", "joint external edge starts to contact" and "EG fully opened". In the hogging moment scenario, the bearing performance can be divided into three stages by the two key points "SG opened" and "EG starts to open".
2. Although the EG can alleviate the concentration of the concrete stress to a certain extent, it has a significant influence on softening the joint, which can lead to the result that the average rotational stiffness and ultimate bearing capacity of the joint with EG are evidently smaller and weaker than those of the segmental joint without EG separately. In addition, with decreasing the axial force, this softening effect tends to be more obvious. Therefore, it is necessary to fully consider the influence of EG on the joint rotational stiffness and ultimate bearing capacity during the design of segment lining, or it will lead to dangerous design situations.
3. Whether for the joint with EG or for the joint without EG, with increasing the bending moment, the concrete at joint edges yields firstly, then the rate of the joint opening increases rapidly, and finally, it leads to bolt yield and joint failure. Therefore, during the production, transportation and assembly of the segments, enough attention should be paid to the protection of the concrete at the joint edges. If necessary, increasing the strength of the corresponding concrete will be an effective way to improve the ultimate bearing capacity of the segmental joint.

Acknowledgment

This work is supported by the Fundamental Research Funds for the Central Universities (No. JZ2022HGTA0335, No. JZ2021HGTA0097).

[3] Yang, T., Ma, J. "Intelligent water scheme design based on artificial intelligence, internet of things and big data technology", In: Guan, M., Na, Z. (eds.) *Machine Learning and Intelligent Communications*, 5th International Conference, MLICOM 2020, Springer, 2021, pp. 424–428. ISBN 978-3-030-66784-9 https://doi.org/10.1007/978-3-030-66785-6_46

[4] Cho, S. H., Kim, J., Won, J., Kim, M. K. "Effects of jack force and construction steps on the change of lining stresses in a TBM tunnel", *KSCE Journal of Civil Engineering*, 21, pp. 1135–1146, 2017. <https://doi.org/10.1007/s12205-016-0391-y>

- [5] Luciani, A., Peila, D. "Tunnel waterproofing: available technologies and evaluation through risk analysis", *International Journal of Civil Engineering*, 17, pp. 45–59, 2019.
<https://doi.org/10.1007/s40999-018-0328-6>
- [6] Zhang, W., Wang, B., Zhang, G. "The influence of dislocation on the stress and waterproof performance of shield tunnel joint", *Chinese Civil Engineering Journal*, 53(S1), pp. 63–68, 2020. (in Chinese)
<https://doi.org/10.15951/j.tmgcxb.2020.sl.011>
- [7] Lee, K. M., Hou, X. Y., Ge, X. W., Tang, Y. "An analytical solution for a jointed shield-driven tunnel lining", *International Journal for Numerical and Analytical Methods in Geomechanics*, 25(4), pp. 365–390, 2001.
<https://doi.org/10.1002/nag.134>
- [8] Ding, W. Q., Yue, Z. Q., Tham, L. G., Zhu, H. H., Lee, C. F., Hashimoto, T. "Analysis of shield tunnel", *International Journal for Numerical and Analytical Methods in Geomechanics*, 28(1), pp. 57–91, 2004.
<https://doi.org/10.1002/nag.327>
- [9] Do, N.-A., Dias, D., Oreste, P., Djeran-Maigre, I. "2D numerical investigation of segmental tunnel lining behavior", *Tunnelling and Underground Space Technology*, 37, pp. 115–127, 2013.
<https://doi.org/10.1016/j.tust.2013.03.008>
- [10] Working Group No. 2, International Tunnelling Association "Guidelines for the design of shield tunnel lining", *Tunnelling and Underground Space Technology*, 15(3), pp. 303–331, 2000.
[https://doi.org/10.1016/S0886-7798\(00\)00058-4](https://doi.org/10.1016/S0886-7798(00)00058-4)
- [11] Zhu, H. H., Huang, B. Q., Li, X. J., Hashimoto, T. "Unified model for internal force and deformation of shield segment joints and experimental analysis", *Chinese Journal of Geotechnical Engineering*, 36(12), pp. 2153–2160, 2014. (in Chinese)
<https://doi.org/10.11779/CJGE201412001>
- [12] Li, X., Yan, Z., Wang, Z., Zhu, H. "A progressive model to simulate the full mechanical behavior of concrete segmental lining longitudinal joints", *Engineering Structures*, 93, pp. 97–113, 2015.
<https://doi.org/10.1016/j.engstruct.2015.03.011>
- [13] Feng, K., He, C., Qiu, Y., Zhang, L., Wang, W., Xie, H., Zhang, Y., Cao, S. "Full-scale tests on bending behavior of segmental joints for large underwater shield tunnels", *Tunnelling and Underground Space Technology*, 75, pp. 100–116, 2018.
<https://doi.org/10.1016/j.tust.2018.02.008>
- [14] Liu, H., Liu, H. "Numerical investigation on the mechanical behaviour of shield tunnel segment and their longitudinal joint", *Chinese Journal of Underground Space and Engineering*, 15(6), pp. 1800–1810, 2019. (in Chinese)
- [15] Zhang, L., Su, R., He, C., Feng, K., Fang, R., Xu, P. "Full-scale experimental study on bending performance of segmental joints of large cross-section shield tunnel under pure compressive bending condition", *Tunnel Construction*, 40(7), pp. 997–1003, 2020. (in Chinese)
<https://doi.org/10.3973/j.issn.2096-4498.2020.07.008>
- [16] Zhang, H., Guo, C., Fu, D. "A study on the stiffness model of circular tunnel prefabricated lining", *Chinese Journal of Geotechnical Engineering*, (3), pp. 309–313, 2000. (in Chinese)
<https://doi.org/10.3321/j.issn:1000-4548.2000.03.009>
- [17] Jiang, H., Hou, X. "Theoretical study of rotating stiffness of joint in shield tunnel segments", *Chinese Journal of Rock Mechanics and Engineering*, (9), pp. 1574–1577, 2004. (in Chinese)
<https://doi.org/10.3321/j.issn:1000-6915.2004.09.030>
- [18] Xia, C., Zeng, G., Bian, Y. "Method for determining bending stiffness of shield tunnel segment rings longitudinal joint based on fix-point iteration", *Chinese Journal of Rock Mechanics and Engineering*, 33(5), pp. 901–912, 2014. (in Chinese)
- [19] Yang, F., Cao, S., Qin, G. "Simplified spring models for concrete segmental lining longitudinal joints with gaskets", *Tunnelling and Underground Space Technology*, 96, 103227, 2020.
<https://doi.org/10.1016/j.tust.2019.103227>
- [20] Zhong, X., Zhu, W., Huang, Z., Han, Y. "Effect of joint structure on joint stiffness for shield tunnel lining", *Tunnelling and Underground Space Technology*, 21(3-4), pp. 407–408, 2006.
<https://doi.org/10.1016/j.tust.2005.12.215>
- [21] Cavalaro, S. H. P., Aguado, A. "Packer behavior under simple and coupled stresses", *Tunnelling and Underground Space Technology*, 28, pp. 159–173, 2012.
<https://doi.org/10.1016/j.tust.2011.10.008>
- [22] Zhang, J., He, C. "Analysis on mechanical properties of segment joints with different pressure pads", *Journal of the China Railway Society*, 35(12), pp. 101–105, 2013. (in Chinese)
<https://doi.org/10.3969/j.issn.1001-8360.2013.12.016>
- [23] Ministry of Housing and Urban-Rural Construction of the People's Republic of China "GB 50010 Code for design of concrete structures", Beijing, China, China Architecture and Building Press, 2010. (in Chinese)
- [24] Zhang, J., Li, W. "Research on key issues of improved strip algorithm for segmental joints", *Journal of the China Railway Society*, 42(3), pp. 147–152, 2020. (in Chinese)
<https://doi.org/10.3969/j.issn.1001-8360.2020.03.018>
- [25] Arnau, O., Molins, C. "Three dimensional structural response of segmental tunnel linings", *Engineering structures*, 44, pp. 210–221, 2012.
<https://doi.org/10.1016/j.engstruct.2012.06.001>
- [26] Zhao, W., Chen, W., Yang, F. "Study of the interface mechanical properties of concrete segments in shield tunnels", *Modern Tunnelling Technology*, 52(3), pp. 119–126, 2015. (in Chinese)
<https://doi.org/10.13807/j.cnki.mtt.2015.03.017>
- [27] Gong, C., Ding, W., Mosalam, K. M., Günay, S., Soga, K. "Comparison of the structural behavior of reinforced concrete and steel fiber reinforced concrete tunnel segmental joints", *Tunnelling and Underground Space Technology*, 68, pp. 38–57, 2017.
<https://doi.org/10.1016/j.tust.2017.05.010>
- [28] Avnaki, M. J., Hoseini, A., Vandani, S., de la Fuente, A. "Numerical-aided design of fiber reinforced concrete tunnel segment joints subjected to seismic loads", *Construction and Building Materials*, 170, pp. 40–54, 2018.
<https://doi.org/10.1016/j.conbuildmat.2018.02.219>
- [29] Zhang, L., Feng, K., Li, M., Sun, Y., He, C., Xiao, M. "Analytical method regarding compression-bending capacity of segmental joints: theoretical model and verification", *Tunnelling and underground space technology*, 93, 103083, 2019.
<https://doi.org/10.1016/j.tust.2019.103083>
- [30] Qiu, Y., Hu, X., Walton, G., He, C., He, C., Woody Ju, J. "Full scale tests and a progressive failure model to simulate full mechanical behavior of concrete tunnel segmental lining joints", *Tunnelling and Underground Space Technology*, 110, 103834, 2021.
<https://doi.org/10.1016/j.tust.2021.103834>